Philosophical Magazine

ISSN: (Print) (Online) Journal homepage: www.tandfonline.com/journals/tphm20

A self-excitation point process model for quantifying nanoparticle agglomeration

Samarth Motagi, James Harris, Alberto Mello, Foram Madiyar & Sirish Namilae

To cite this article: Samarth Motagi, James Harris, Alberto Mello, Foram Madiyar & Sirish Namilae (14 Jul 2024): A self-excitation point process model for quantifying nanoparticle agglomeration, Philosophical Magazine, DOI: 10.1080/14786435.2024.2374530

To link to this article: https://doi.org/10.1080/14786435.2024.2374530

PHILOSOPHICAL MAGAZINE
https://doi.org/10.1080/14786435.2024.2374530

Taylor & Francis
Taylor & Francis Group

A self-excitation point process model for quantifying nanoparticle agglomeration

Samarth Motagi, James Harris, Alberto Mello, Foram Madiyar and Sirish Namilae

Department of Aerospace Engineering, Embry-Riddle Aeronautical University, Daytona Beach, FL, USA

ABSTRACT

Nanoparticle agglomeration refers to the spontaneous clustering of nanoparticles caused by the attractive forces. Agglomeration impacts the physical and mechanical properties of nanoparticles and their composites. Understanding and controlling nanoparticle agglomeration is crucial for optimizing various applications, from nanomedicine to nanoelectronics. In this work, we formulated a self-exciting point process model to analyse nanoparticle agglomeration based on microstructural input. The model is utilised to categorise a specific set of points within the microstructure as either independent (dispersed) or dependent (agglomerated), along with their respective probabilities. We employed this approach to study two distinct scenarios: (a) Agglomeration in experimentally generated microstructures of titanium nanoparticles, and (b) Analysing agglomeration patterns in simulated microstructures of carbon nanotube networks, generated using a stochastic microstructure model. We obtain a quantitative understanding of the connection between the sonication duration and the level of agglomeration in titanium nanoparticles. As the sonication period increases, both the agglomeration percentage and the size of the agglomerates decrease. Furthermore, our analysis of simulated carbon nanotube microstructures, including equiaxed and rope-like agglomeration, shows a close alignment between results obtained from the point process model and those generated by the stochastic microstructure model.

ARTICLE HISTORY
Received 20 October 2023
Accepted 19 June 2024

KEYWORDS
Nanoparticle agglomeration; self-excitation point process model; titanium nanoparticles; carbon nanotubes

1. Introduction

Nanoparticles often possess distinct physical and chemical characteristics that differ from bulk materials, giving rise to unique behaviours. Agglomeration is one such phenomenon where nanoparticles come together, forming larger assemblies through spontaneous clustering or aggregation. The different factors that contribute to nanoparticle agglomeration, include van der Waals

CONTACT Sirish Namilae email-namilaes@erau.edu Department of Aerospace Engineering, Embry-Riddle Aeronautical University, Daytona Beach, FL, USA

forces, electrostatic interactions, surface chemistry, solvent effects, and external factors like temperature and pH [1–4]. Agglomeration of nanoparticles leads to several outcomes, including reduced surface area [5], altered optical properties [6], change in mechanical properties [7], and loss of homogeneity [8].

Various characterisation methods have been used to study nanoparticle agglomeration, such as dynamic light scattering [9], transmission electron microscopy (TEM) [10], scanning electron microscopy (SEM) [11], atomic force microscopy (AFM) [12], and spectroscopic methods [13]. Verleysen et al. [14] employed a quantitative approach for assessing stable dispersions, which involves TEM imaging in conjunction with semi-automated image analysis. This methodology yields number-based distributions of key parameters, allowing for the measurement of size, shape, and surface characteristics of TiO_2 particles in their unbound, aggregated, and agglomerated states. Rao et al. [15] employed AFM to analyse the morphology, dimensions, and size distribution of various ceramic nanoparticle agglomerates. Jia et al. [16] performed real-time sizing during the colloidal processing of metal oxide nanoparticles (MONs) using dynamic light scattering.

Modelling of nanoparticle agglomeration involves mathematical or computational approaches to simulate how nanoparticles cluster together, considering factors like size, shape, surface charge, environmental conditions, and external forces. Models often based on stochastic methods are used to understand agglomeration kinetics, predict agglomerate size distributions, and assess nanoparticle dispersion stability. Kim et al. [17] investigated the aggregation kinetics of gold nanoparticles through a combination of experimental methods and Monte Carlo simulations. This study predicts the time needed for the initial color change in a gold nanoparticle suspension, offering insights into the design and optimisation of colorimetric sensors utilizing gold nanoparticle aggregation. Liu et al. [18] applied a constant-number Direct Simulation Monte Carlo (DSMC) model to study nanoparticle agglomeration in aqueous suspensions. They used classical Derjaguin–Landau–Verwey–Overbeek (DLVO) theory, factoring in Brownian motion's effect on collision frequency. The model's outcomes aligned closely with dynamic light scattering measurements for particle size distribution and average agglomerate size. Morán et al. [19] introduce a new method to enhance the accuracy of Monte Carlo simulations for predicting dynamics and agglomeration of suspended nanoparticles. This approach incorporates persistent distance and time steps based on Langevin dynamics simulations and a probability model for particle displacements. Gbaguidi et al. [20,21] employed a two-dimensional Monte Carlo percolation model to investigate the impact of carbon nanotube (CNT) agglomeration on the electrical and electromechanical properties of both monofiller and hybrid nanocomposites. Bhoi et al. [22] developed a mathematical population balance model to characterize the evolution of Al_2O_3 nano-agglomerates

in a spouted bed. Agglomeration process is simulated using an Equipartition of Kinetic Energy (EKE) kernel, signifying the equal distribution of kinetic energy among particles, enabling collective formation into agglomerates. In contrast, for breakage, two distinct functions are employed: the Dirac delta function indicating immediate and concentrated particle breakage, and a function representing confined uniform binary breakage, where particles break into fragments with a uniform size distribution. The model exhibits good agreement with experimental observations concerning the temporal evolution of both the area and volume-weighted average sizes of nano-agglomerates, as well as their final size distribution.

In addition to stochastic methods, approaches like Molecular Dynamics have been used to understand the interparticle forces that contribute to agglomeration. Liao et al. [23] employed molecular dynamics simulations to investigate the factors that impact the formation of agglomeration structures in Cu–Ar nanofluids. Wang et al. [24] conducted equilibrium molecular dynamics simulations and the Schmidt–Ott equation to analyse the fractal dimensions of the nanoparticle aggregations with various morphologies. The findings suggested that achieving lower fractal dimensions can lead to enhanced thermal conductivity. Alian et al. [25] conducted molecular dynamic simulations that considered both the curvature and agglomeration of carbon nanotubes to analyse their influence on the interfacial strength and load transfer capacity in thermoset nanocomposites.

In this study, we introduce a new approach based on point process modelling to analyse nanoparticle agglomeration. A point process model is a statistical framework used to describe and analyse the spatial or temporal distribution of points or events in a particular region or over a specific period. Hawkes process, also known as self-exciting point process, is a branching point process model [26]. It describes a random sequence of clustered events or points wherein the presence of one point (or event) increases the likelihood of subsequent points (or events) occurring in its spatial or temporal vicinity. While the application of self-exciting point process models originated in the field of earthquake analysis to categorise mainshock and aftershock events from earthquake data, it has found applications across diverse domains. These domains include crime event analysis [27], tweet popularity prediction [28], epidemiological studies [29], as well as the analysis of instances involving mass killings and school shootings [30], email network [31], and financial data analysis [32].

The Hawkes process is parameterised by two functions, the background intensity, which describes the average rate of occurrence of events in the absence of any previous events. The excitation function, which describes how the occurrence of an event affects the probability of subsequent events. The parameters of self-exciting point process models can be estimated from data. This allows the models to be used to make predictions about future

events. Self-exciting point process models are a powerful tool for analysing sequences of events. They have been used to make significant contributions to a wide range of fields.

Hawkes point process model used in this study has the ability to capture spatial and temporal clustering, account for intensity variation, and facilitate statistical inference and prediction. Therefore, these models offer a novel statistical framework that can analyse the characteristics of agglomeration processes, making it a potentially effective approach. While this model has not yet been used in materials science and can bring a fresh perspective and could possibly be adapted to other similar materials science problems.

We apply this approach to analyse nanoparticle agglomeration in two distinct contexts: (a) experimentally generated microstructures of titanium nanoparticles, and (b) simulated microstructures of carbon nanotube agglomeration derived from a stochastic microstructure model. Experimental micrographs of titanium nanoparticles with various degrees of agglomeration were achieved by subjecting solutions with the same concentration to different durations of ultrasonic treatment. Simulated CNT microstructures exhibiting a range of agglomeration patterns for carbon nanotubes, including both equiaxed and rope-like morphologies were obtained using a stochastic microstructure model. Using these micrographs, we extracted the nanoparticle locations and applied a point process model to analyse the nanoparticle agglomeration. Our findings indicate that the point process model is an effective tool for analysing agglomeration and holds potential for further applications in nucleation-growth processes in materials science.

2. Methodology

2.1. Generation of experimental microstructures

99.9% pure spherical titanium nanoparticles – product number 1121XH from SkySpring Nanomaterials Inc., were procured for utilisation in this study. To prepare the nanoparticle solution, 0.001 g of titanium nanoparticle powder was combined with 8 ml of isopropyl alcohol (IPA), resulting in a solution with a concentration of 0.125 mg/ml. The SCILOGEX MX-T6-S Analog Tube Roller was employed to disperse titanium nanoparticles in the solution and reduce agglomeration. The nanoparticle solution inside a vial with SiC balls was placed within the tube roller for 24 h, operating at a speed of 50 rpm, effectively breaking apart the nanoparticle clusters and reducing the size of the agglomerates. Additionally, ultrasonication is employed to further break apart the nanoparticle agglomerates. Ultrasonication produces high-frequency sound waves within the liquid medium, resulting in the formation of pressure waves and cavitation bubbles. As these bubbles collapse, they generate micro-turbulence and shear forces, effectively dispersing and breaking the agglomerated nanoparticles [33]. Consequently, ultrasonication facilitates the

even distribution of nanoparticles throughout the liquid medium, serving as an effective measure to prevent or reduce agglomeration. Different levels of agglomeration were achieved by subjecting individual solutions to ultrasonic treatment for different durations with 5, 10, 20, 30, 60, 90 and 120 min. Subsequently, 40 µl droplets of each solution were dispersed onto an epoxy polymer substrate using a micro-pipette. The solution was immediately deposited onto the substrate within a minute of ultrasonication to prevent reagglomeration. To facilitate solvent evaporation, the prepared samples were subjected to a temperature of 50°C using an Aluminium top hotplate. The resulting micrographs displayed differing levels of nanoparticle agglomeration in the samples. Notably, the application of one hour or more of ultrasonic treatment duration was correlated with the uniform dispersion of the nanoparticles across the sample. Conversely, shorter durations of ultrasonic treatment resulted in a more noticeable agglomeration in the samples, as shown in Figure 1. When the as-prepared nanoparticle solution without sonication is used to generate microstructures, large agglomerates are present.

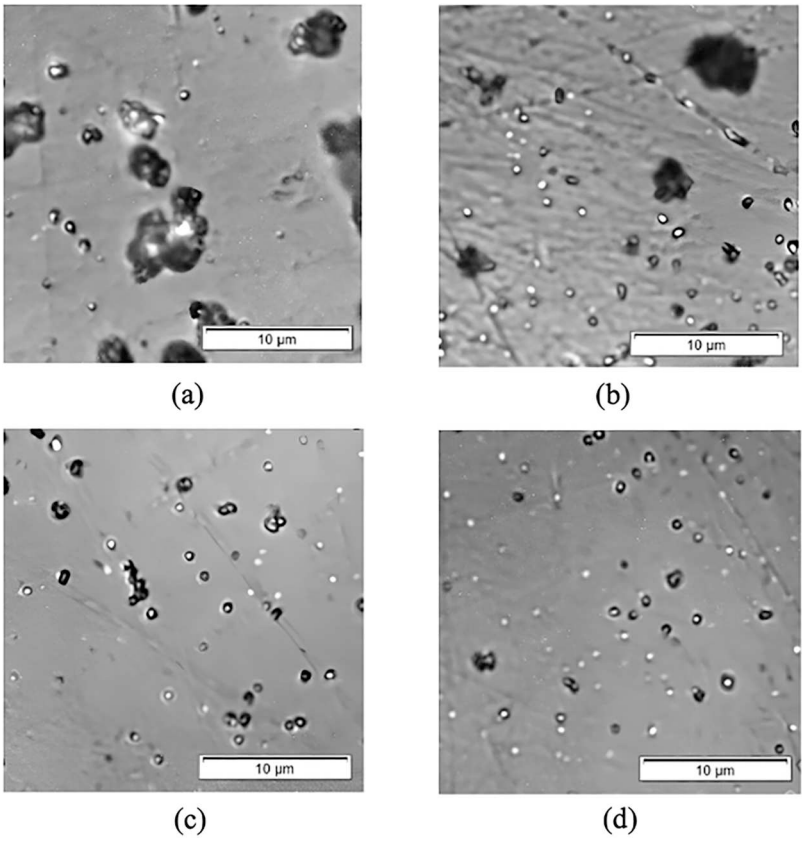

Figure 1. Titanium nanoparticles dispersed on the substrate at different sonication times (a) 5 min (b) 30 min (c) 1 h and (d) 2 h.

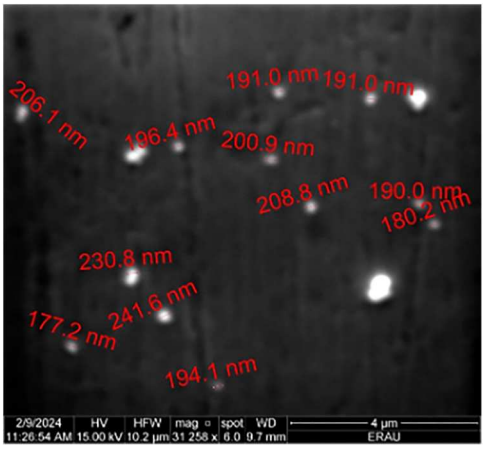

Figure 2. SEM micrograph of the nanoparticles after ultrasonication for 120 min.

The agglomerates reduce in size with increasing sonication duration. Additional sonication time did not reduce the particle size further. This particle size is measured using dynamic light scattering (DLS) measurements. After two hours of sonication, we observe that particles of about 200 nm size and are uniformly distributed.

We performed SEM micrographic analysis to further characterise the particle size distribution after ultrasonication for 120 min as shown in Figure 2. Scanning electron microscopy ascertained that the average particle size of titanium nanoparticles is 197 nm. Particle size is also confirmed using Dynamic Light Scattering – Malvern Zetasizer ZS90 to measure the size of particles in an IPA solution at 25°C. The technique relies on analysing the fluctuations in light scattering intensity caused by the Brownian motion of particles suspended in a liquid. By analysing the intensity fluctuations, DLS can determine the size of the particles in the solution, typically in the range of a few nanometres to a few micrometres. After 120 min of ultrasonication, the DLS measurements recorded a particle size of 195.37 nm and a zeta potential of −32.5 mV. This closely matches SEM analysis.

2.2. Generation of simulated microstructures

Simulated microstructures of agglomerated CNTs were generated using a stochastic microstructural model. These CNTs were generated within a Representative Area Element (RAE) with dimensions (L_x and L_y). Each CNT took the form of a line segment with a midpoint (x_{ic}, y_{ic}), a starting point (x_1^i, y_1^i), and an endpoint (x_2^i, y_2^i). Additionally, the length and polar angle of each CNT were represented by l_i and $Ø_i$, respectively. Different microstructures are generated by stochastically varying all of these parameters, simulating the complexity found in real-world microstructures. To calculate the volume fraction, all the

CNTs in the RAE are assumed to have a uniform diameter D_{CNT}. The CNT volume fraction is defined as the ratio of the total volume encompassed by all the CNTs ($\pi \times r_0^{i2} \times l_i$) to the area of the RAE ($L_x \times L_y$). To achieve the desired CNT volume fraction, nanotubes were added to the RAE until the specified volume fraction was attained. The centre of each CNT consistently falls within the confines of the RAE. In some instances, CNTs may intersect with one or even both edges of the RAE. To handle this situation, we employed periodic boundary conditions. These conditions efficiently relocated any line segments that extended beyond the RAE's boundaries, placing them on the opposite side of the RAE to ensure that they always remained contained within the RAE. The microstructure generation is described in detail in [34].

We modify this approach to generate microstructures featuring different quantities and morphologies of CNT agglomerates. This process begins with the generation of a seed layer consisting of completely randomised and uniformly distributed fillers. Subsequently, we introduce additional fillers in a manner that results in the formation of agglomerates around a portion of the initial seed layer. The total volume fraction of CNTs (V_f) within the RAE is determined by summing the volume fractions of both agglomerated (V_f^{agg}) and non-agglomerated CNTs $(V_f^{non-agg})$. The agglomeration level or volume fraction of agglomeration is then modelled by $\xi_{agg} = V_f^{agg}/V_f$. Two distinct microstructural configurations were generated by varying parameters related to agglomeration: the rope-like and equiaxed agglomerates. The formation of these structures was governed by two key parameters, ξ_{agg} and α_{agg}. The agglomeration parameter, ξ_{agg}, dictated the proportion of CNTs that were organised into agglomerates. For instance, when $\xi_{agg} = 0$, CNTs are uniformly distributed throughout the representative area element without any agglomeration. As ξ_{agg} increased, the degree of agglomeration increased. When $\xi_{agg} =$ 10%, in the first step the CNTs are uniformly distributed throughout the RAE without any agglomeration and then the additional small fraction of CNT fillers is added which results in the formation of agglomerates. Similar, procedure is carried out for varying levels of CNT agglomeration. The agglomeration angle, α_{agg}, is used to model the spatial arrangement of CNTs within an agglomerate. The newly added CNTs are positioned at a randomly varied angle between 0 and α_{agg} with respect to one of the pre-existing CNTs in the microstructure. When $\alpha_{agg} = 0°$, CNTs within an agglomerate are all aligned in parallel, resulting in the formation of rope-like agglomerates within the microstructure. Conversely, when $\alpha_{agg} = 180°$, CNTs within an agglomerate exhibit varied orientation, giving rise to equiaxed or star-like agglomerate formations. Figure 3 (a) and (b) illustrated microstructures showcasing the equiaxed and rope-like agglomerates, respectively, with agglomeration level of 50%. These details are presented in detail in [21]. For each agglomeration level, 25 microstructures were generated from the stochastic model to account for statistical variations in the point process agglomeration analysis.

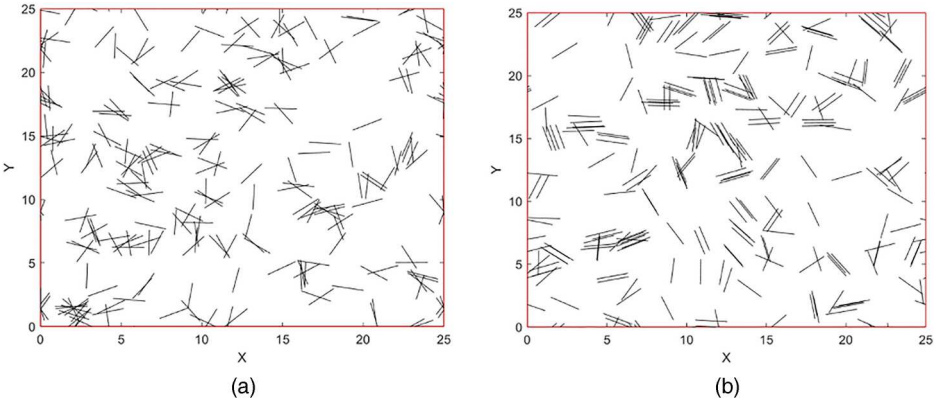

Figure 3. (a) Equiaxed agglomeration and (b) Rope-like agglomeration of carbon nanotubes.

2.3. Point process model formulation for agglomeration analysis

Consider a microstructure that consists of N points which represent the location of nanoparticles. r_i is the distance of a point i from origin.

$$\lambda(r) = \mu + \sum_{i:r_i<r} g_{A,\,\alpha}(r - r_i). \tag{1}$$

Here, λ is the limiting expected distribution of points. The model classifies the nanoparticles in the dataset into two categories, uniformly dispersed nanoparticles and agglomerated nanoparticles. Uniformly dispersed nanoparticles are assumed to be distributed independently at an areal density $\mu > 0$. This model primarily addresses discrete agglomeration state as described by a micrograph at a given location and time.

$g_{A,\alpha}(r - r_i)$ is the probability density function (PDF) of the occurrence of an agglomerated nanoparticle at a distance r_i and is modelled as follows:

$$g_{A,\alpha}(r - r_i) = \begin{cases} A * \alpha * \exp[-\alpha * (r - r_i)], & r > r_i\,, \\ 0 \qquad\qquad\qquad\qquad\quad\;\; , & r \le r_i. \end{cases} \tag{2}$$

The conditional intensity function $\lambda(r|H_r)$ can now be expressed as follows:

$$\lambda(r) = \mu + A \sum_{i:r_i<r} \alpha.e^{-\alpha(r-r_i)}. \tag{3}$$

In this case, α denotes the decay rate in distance for the occurrence of an agglomerated nanoparticle, and A is the preexponential parameter describing the magnitude of excitation. Notably, $g_{A,\alpha}$ is the function that describes the delta $r - r_i$ between an agglomerated and corresponding uniformly dispersed seed nanoparticle. The model is defined by three unknown parameters $\theta = (\mu,\ A,\ \alpha)$. While fitting the model to the microstructure data, these parameters are computed using maximum likelihood estimation. The log-

likelihood function [35] is given a distance series of microstructure data consisting of N points $\{(r_i),\ i = 1, \ldots, N\}$ in an area.

$$l(\theta|H_r) = \sum_{i=1}^{N} log\lambda_\theta(r_i|H_{ri}) - \int_0^R \lambda_\theta(r|H_r)dr. \tag{4}$$

The Davidon–Fletcher–Powell (DFP) approach, a gradient-based nonlinear optimisation procedure, is used to derive the maximum likelihood estimate (MLE) [32]. The DFP method works by iteratively updating an approximation to the inverse Hessian matrix. This approximation is used to generate a search direction, which is then used to update the current estimate of the minimum. The process is repeated until the convergence criteria are met. The probability that point i triggered point j, i.e. the probability that a nanoparticle j is in an agglomerate with nanoparticle i as a seed is given by:

$$p_{ij} = \begin{cases} \dfrac{g_{A,\alpha}(r_j - r_i)}{\lambda(r_j|H_{r_j})} & , r_j > r_i, \\ 0 & , r_j \le r_i. \end{cases} \tag{5}$$

Hence, the probability of nanoparticle j being an agglomerated nanoparticle is $p_j = \sum_{i=1}^{j-1} p_{ij}$. Consequently, the probability of nanoparticle j being a uniformly dispersed nanoparticle is:

$$1 - p_j = \frac{\mu}{\lambda(r_j|H_{r_j})}. \tag{6}$$

Based on the probability values p_j obtained from the model of N nanoparticle points can be classified into uniformly dispersed and agglomerated nanoparticles. This categorisation allows us to compute the microstructure's agglomeration level and the average agglomeration size of nanoparticles in a given microstructure. Pseudocode outlining the algorithm of the Hawkes point process model is shown in Figure 4.

The point process model described above relies on input data consisting of the distances of individual nanoparticles from the origin. To acquire these data, we first need to extract the nanoparticle locations from both experimental and simulated microstructures. We employed a widely used tool WebPlotDigitizer [36] to extract nanoparticle positions from the experimental microstructures. In the case of simulated microstructure, the centre of the CNT location is extracted directly from the model data. Subsequently, we calculated the distance of individual nanoparticle from the origin. This data is used as an input for the point process model.

Two or more nanoparticles at different angles may have the same radial distance from the origin. To avoid the overlapping of such nanoparticles, segments are created to allocate unique locations for the CNTs as shown in Figure 5. If any of the clustered nanoparticles (especially CNTs) are split across segments,

Algorithm: Simulation of Hawkes Point Process Model

1. Extract the location of each of the N nanoparticle in the RAE. (For both experimentally and computationally generated microstructures.)
2. Calculate the distance from the origin (r_i) *for particle i.* Find $\{(r_i), i = 1, \ldots, N\}$.
3. Find background intensity rate $\mu(r)$ corresponding to uniformly distributed microstructure with no agglomerates.
4. Calculate the conditional intensity function $\lambda(r) = \mu + \sum_{i:r_i<r} g_{A,\alpha}(r - r_i)$ in the space interval R= [s_{start}, s_{end}] for a given background intensity $\mu(r)$.
5. **inputs:**
   θ_0 - initial guess for the model parameters $\theta = (\mu, A, \alpha)$
   $\mu(r)$ - background rate
   k - 0
6. **Start loop**
7. use θ_k and get θ_{k+1}
8. $p_i = \frac{\mu}{\lambda(r_j|H_{r_j})}$ - Probability values for uniformly dispersed nanoparticles
9. k = k+1
10. **until** $l(\theta|H_r) = \sum_{i=1}^{N} log\lambda_\theta(r_i|H_{ri}) - \int_0^R \lambda_\theta(r|H_r)dr$ - Maximum Likelihood Estimation is optimized for the model parameters $\theta = (\mu, A, \alpha)$
11. **return** θ_k
12. **Post analysis:** based on the probability values obtained from the model nanoparticles are classified as dispersed (when $p_i < 0.9$) or agglomerated particles (when $p_i > 0.9$)
13. Based on the probability values and particle locations agglomeration levels and agglomerate sizes are quantified for a given microstructure

Figure 4. Pseudocode outlining the algorithm of Hawkes Point Process Model.

then the particles that are closest to one another are forced to fall within the same segment. Figure 5 shows two CNT clusters inside segments 1 and 4; in this example, the nanoparticles are assigned a unique position within their respective segments. In this case, when we see that one cluster is split across two segments (i.e. segments 2 and 3), so we create a buffer segment to ensure that the cluster is not divided across the segments, and any particles that are close by within the buffer segment are considered in the same segment. In this scenario, CNTs are considered in segment 2 and ignored in segment 3 to avoid recurrence. These scenarios are more common for high aspect ratio particles like CNTs.

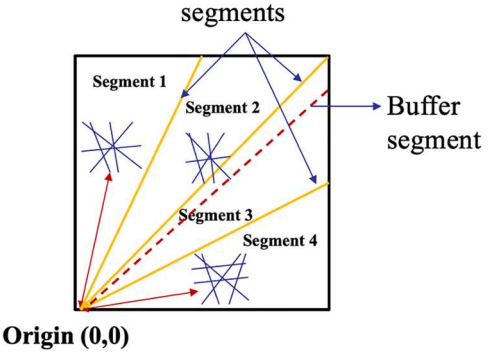

Figure 5. Allocation of unique location to CNTs in a micrograph.

3. Results

3.1. Analysis of experimental microstructures

The digitised nanoparticle positions from the experimental micrographs captured at various sonication times are as shown in Figure 6. Due to the limited contrast between the nanoparticles and the substrate, we used a manual process to extract the nanoparticle locations. However, this process can be easily automated using higher contrast particles. Once we have obtained the nanoparticle location data, we utilise MATLAB code to create segmentation that assigns unique identifiers to these locations as explained in Section 2.3. This dataset is used as input for the point process model, enabling the classification of nanoparticles into two categories: those that are uniformly dispersed and agglomerated nanoparticles.

The point process model provides output in terms of probability values that play a crucial role in classifying nanoparticle behaviour. Equation (5) is used to compute the probability that a given particle is uniformly dispersed. This probability value is the basis for the classification of all points as independent (i.e. dispersed) or dependent (i.e. part of an agglomerate. All agglomerates will still contain one particle that is classified as an independent point and the surrounding particles close to this independent particle would have low probability values indicating that they are a part of the agglomerate. The choice of the probability value 0.8 was determined as a threshold through visual examination, where it was noted that nanoparticles are in an agglomerated state when the probability that they are independent was below 0.8. Figure 7 shows the microstructure of titanium nanoparticles alongside a corresponding contour plot of

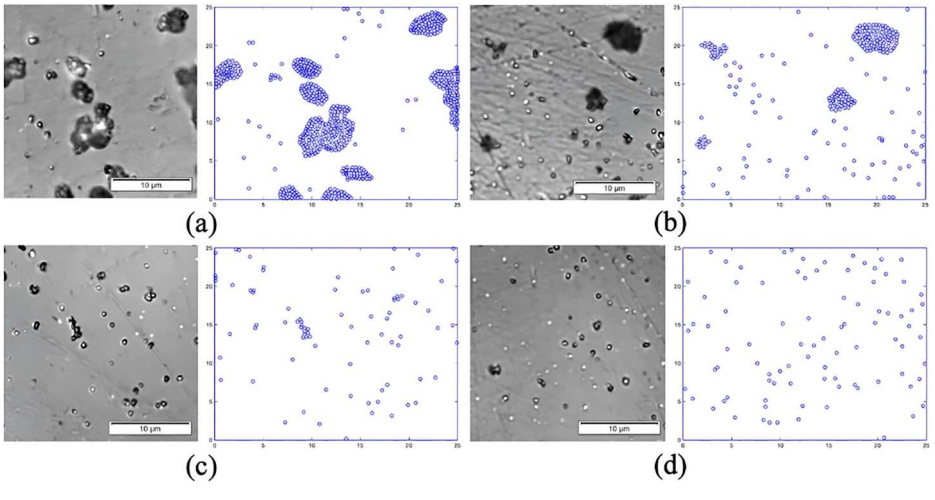

Figure 6. Extracted titanium nanoparticle location dispersed on the substrate at different sonication time (a) 5 min (b) 30 min (c) 1 h and (d) 2 h.

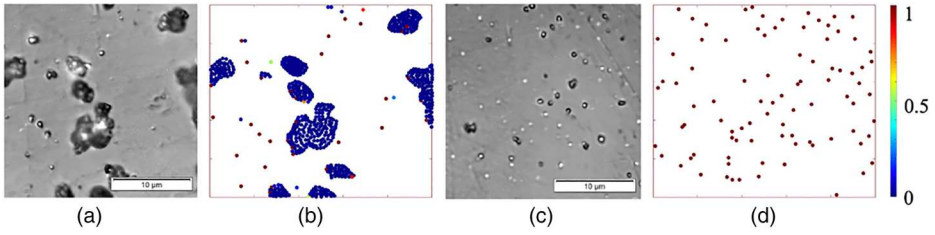

Figure 7. (a) Titanium microstructure sonicated after 5 min, (b) contour plot based on probability values form the model for sonication time 5 min, (c) titanium microstructure sonicated after 2 h and (d) contour plot based on probability values for sonication time 2 h. Note the contour legend corresponds to both (a) and (b), the size of the micrographs is 25 μm × 25 μm.

the probability values. After undergoing 5 min of sonication, the microstructure exhibits a relatively high level of agglomeration. The corresponding contour plot for most particles depicts a low probability that the particles are not agglomerated, indicating high levels of nanoparticle agglomeration. Conversely, the titanium microstructure subjected to 2 h of sonication tends to exhibit much lower levels of agglomeration. In the figure, the corresponding contour plot reveals higher probability values, depicted in red, signifying uniformly dispersed nanoparticles.

We investigated the agglomeration behaviour of titanium nanoparticles in relation to varying sonication durations. Commercially available titanium nanoparticles in a dry powder state are found to be agglomerated into particles that are several hundred nanometres in size [37, 38]. For each specific sonication duration, we capture three micrographs and subsequently quantify the agglomeration percentage based on the probability values generated by the point-process model. The findings presented in Figure 8 illustrate that a higher percentage of titanium nanoparticle agglomeration is observed when sonication times are shorter. It is quite evident that when a shorter duration of ultrasonication was employed, it was insufficient to effectively disperse the nanoparticle agglomerates, consequently resulting in a higher agglomeration percentage. As we progress from sonication duration A to G (see Figure 7), the agglomeration percentage consistently decreases indicating that a higher duration of ultrasonication results in uniform dispersion of the nanoparticles. The error bars depicted in Figure 7 signify the standard deviation of the nanoparticle agglomeration percentage corresponding to each sonication duration. This trend signifies that the nanoparticle agglomerates gradually break apart as the sonication time extends. The model can effectively capture the dynamic relationship between sonication duration and titanium nanoparticle agglomeration.

Once the nanoparticle classification as dispersed or agglomerated particles is completed, we employ a post-processing MATLAB code to determine the size of the nanoparticle agglomerate. This is accomplished by identifying

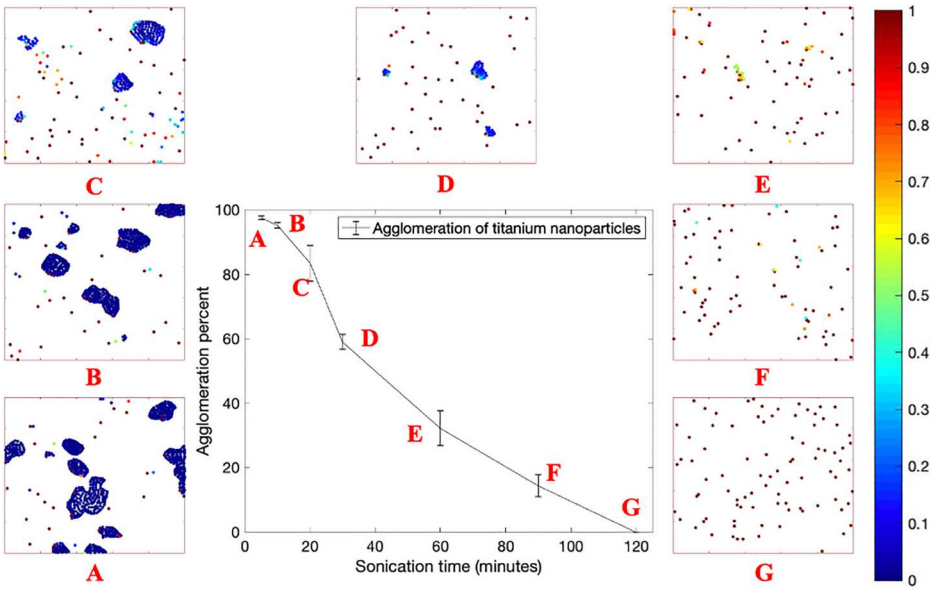

Figure 8. Agglomeration of titanium nanoparticles with respect to sonication time. Note the contour legend corresponds from A to G micrographs and the size of the micrographs is 25 μm × 25 μm.

agglomerate boundary based on the aforementioned probability values. Given that our input data consists of a sequential series of nanoparticle distances from the origin. We use the probability values to identify continuous sequences of values that consistently fall below 0.8. This pattern of consecutive low values is indicative of the existence of nanoparticle clusters. In contrast, if the values remain consistently above 0.8, it signifies that the nanoparticles are uniformly dispersed. By adopting this method, we can pinpoint nanoparticle agglomerate clusters and calculate the size of a given agglomerate, and the average agglomeration size for the micrograph. In Figure 9, as we progress from point A to point F, corresponding to increasing sonication times, it becomes evident that the agglomeration size consistently decreases. This observation indicates the gradual breakdown of nanoparticle agglomerates in response to longer sonication times.

To validate the point process model results, we compared the point process agglomeration analysis with microstructural analysis. The agglomeration statistics were manually extracted from the same micrographs that were used for point process analysis. The comparison between the two approaches shown in Table 1 indicates that point process model accurately captures the agglomeration behaviour.

3.2. Analysis of simulated microstructures

The same methodology is applied to the simulated microstructures containing carbon nanotubes, generated within a Representative Area Element measuring

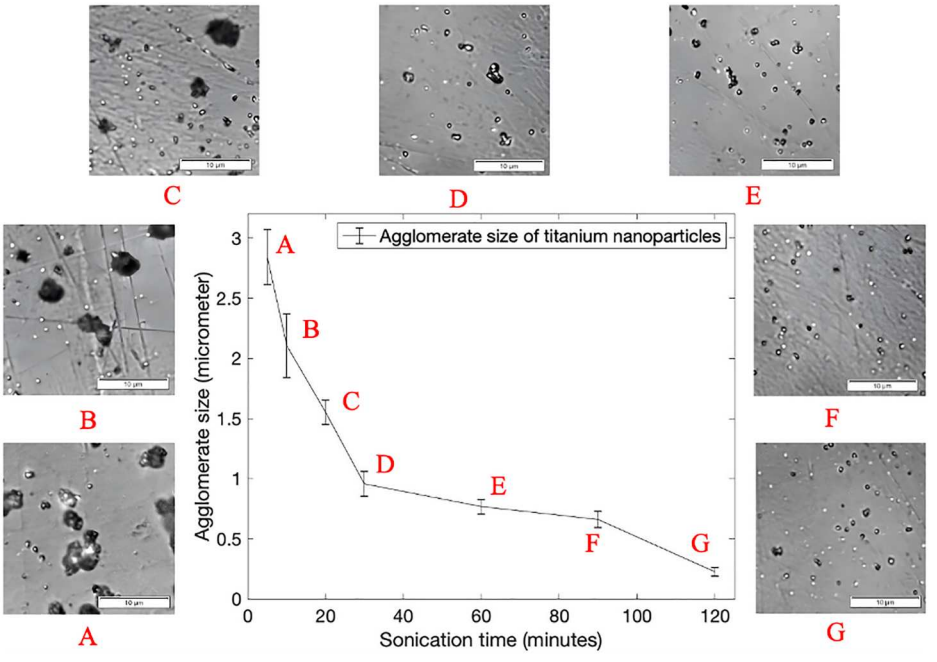

Figure 9. Agglomerate size of titanium nanoparticles with respect to sonication time.

25×25 micrometres. In Figure 10, we present a randomly generated microstructure, featuring a 50% agglomeration of CNT nanoparticles. We can discern two distinct nanoparticle behaviours as depicted in the figure. First, we observe CNT nanoparticle entanglement, which is referred to as agglomerated nanoparticles. Second, there are uniformly dispersed CNT nanoparticles, which appear isolated without nearby CNTs or entanglements. To distinguish between these two behaviours, we utilise a point-process model to calculate probability values for the classification. The corresponding contour plot in Figure 10 represents these nanoparticles based on the probability values obtained from the model. Equation (5) serves as the probability equation for uniformly dispersed nanoparticles, forming the foundation for classification. When the value derived from this equation is below 0.8, it indicates that the nanoparticles are in an agglomerated state. Conversely, when the value

Table 1. Comparison of point process results with manual microstructural analysis in terms of agglomerate size.

Ultrasonication time	Microscopic analysis Mean agglomerate size	Point process analysis Mean agglomerate size	% Difference
5 min	2939 nm	2842 nm	3.3
10 min	1009 nm	956 nm	5.2
1 h	744 nm	768 nm	−3.2
2 h	199 nm	226 nm	−13.56

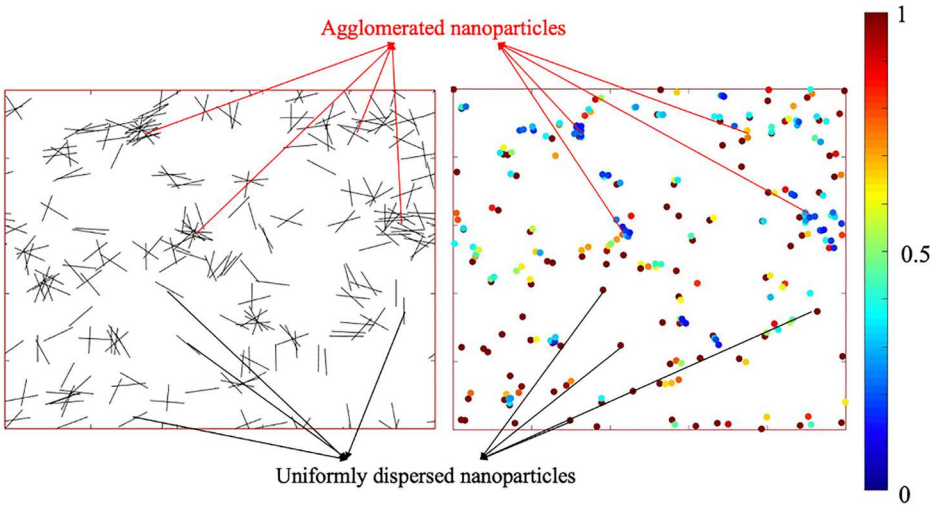

Figure 10. Randomly generated microstructure with 50% agglomeration of CNT nanoparticles and contour plot of representation of nanoparticles based on probability values obtained from point-process model.

exceeds 0.8, it signifies uniform dispersion of the nanoparticles. Uniformly dispersed nanoparticles are depicted as orange to red nanoparticles in the contour plot. In contrast, agglomerated nanoparticles are represented as yellow to blue dots in the contour plot. This approach allows us to effectively differentiate between uniformly dispersed and agglomerated CNT nanoparticles within the simulated microstructure, which helps to quantify nanoparticle agglomeration characteristics.

3.2.1. Equiaxed vs. rope-like agglomerated microstructures

Based on the processing conditions, agglomerates in carbon nanotubes have been found to exhibit two types of morphologies: equiaxed [39, 40] and rope-like [41, 42]. Equiaxed agglomeration of carbon nanotubes refers to a specific clustering pattern of CNTs where the agglomerates take on spherical or star-like shapes. In Figure 11, we can see that the simulated microstructure transitions from uniformly dispersed CNTs to various levels of equiaxed agglomerated microstructures, and this transformation is achieved using a stochastic microstructure model. To quantify these changes, corresponding contour plots represent the probability that a given CNT is in a dispersed state. These values are derived from a point process model. In the first micrograph (a), where CNTs are uniformly dispersed, the probability values are close to 1. This signifies that the CNTs are evenly distributed throughout the microstructure with minimal clustering. As we progress to micrographs (b), (c), and (d), we observe a decrease in probability values, indicating higher levels of agglomeration in the micrographs. In (b), with 30% agglomeration, some

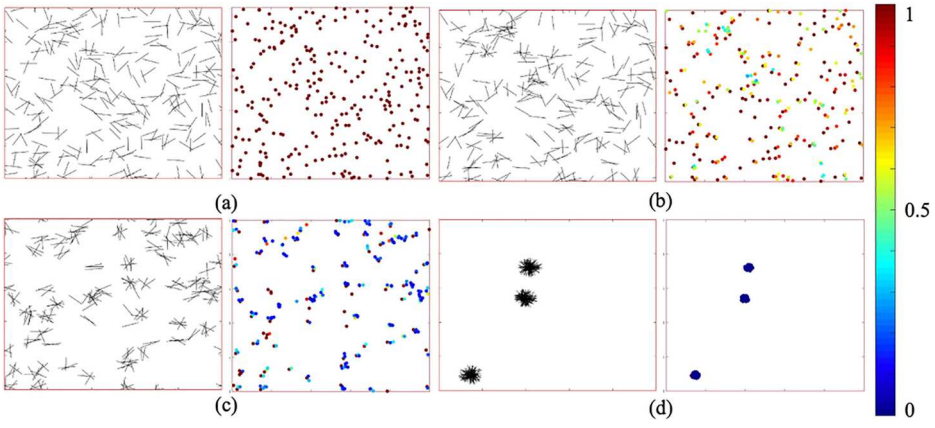

Figure 11. Randomly generated microstructure and contour plot of CNT nanoparticles based on probability values (a) 0% agglomeration (b) 30% agglomeration (c) 70% agglomeration and (d) 99% agglomeration. Note that the size of the micrographs is 25 μm × 25 μm.

clustering of CNTs has begun to occur. In (c), with 50% agglomeration, the clustering becomes more pronounced. Finally, in (d), with 99% agglomeration, the probability value is at its lowest, signifying that a significant portion of CNTs has aggregated into equiaxed agglomerates, forming spherical or star-like structures.

In contrast to equiaxed agglomeration, rope-like agglomeration of carbon nanotubes refers to bundling together CNTs parallel to each other into structures that resemble ropes or fibres. Figure 14 shows the evolution of the simulated rope-like microstructures, varying from uniformly dispersed to increasing levels of rope-like agglomeration. These variations are obtained by changing the input parameters to the stochastic microstructure model as described in Section 2.2. Figure 12 displays simulated micrographs and corresponding contour plots indicating the probability of CNT dispersion. For the completely dispersed state shown in Figure 12 (a), the probability values are close to 1. This signifies that the point process model computes that the CNTs are uniformly distributed throughout the microstructure, with minimal clustering. Figure 10b–d presents micrographs with increasing agglomeration and corresponding probability contours. For both rope-like and equiaxed agglomerated microstructures, the point process model computes the dispersion probabilities effectively which are used for further analysis.

We employed the point process model to categorise nanoparticle distributions as either uniformly dispersed or agglomerated and used this information to quantify the level of agglomeration within a given microstructure. We analysed 25 microstructures of specific agglomeration characteristics to account for statistical variation. We find that the results independently obtained from the point process model closely align with the input parameters used by the stochastic microstructure model to model the microstructures.

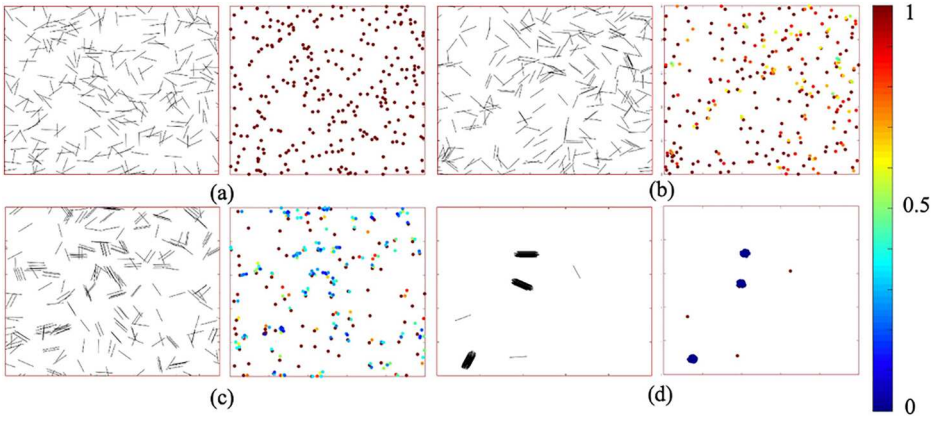

Figure 12. Rope-like generated microstructure and contour plot of CNT nanoparticles based on probability values (a) 0% agglomeration (b) 30% agglomeration (c) 70% agglomeration and (d) 99% agglomeration.

Error bars represent the standard deviation associated with the nanoparticle agglomeration percentages. Figure 13 shows these results for equiaxed microstructure and similar results for rope-like microstructures are shown in Figure 14.

3.2.2. Agglomerate size variation

We utilised the same post-processing MATLAB code used for experimental microstructures, to analyse the size of the nanoparticle agglomerates for the simulated microstructures as well. Figure 15 presents the average agglomerate size for a given agglomeration percentage for both equiaxed and rope-like microstructures. For equiaxed and rope-like agglomerates, the agglomeration size consistently increases with a corresponding rise in the agglomeration percentage. The equiaxed agglomerate exhibits a larger agglomerate size compared to the rope-like agglomerate. This size difference arises from the distinctive star-like shape found in equiaxed agglomerates, whereas rope-like agglomerations are characterised by their fiber-like structure. The reduction in agglomeration size in the rope-like formation is attributed to the alignment of carbon nanotubes, causing a decrease in size along the radial direction. This alignment results in an overall decrease in agglomeration size at higher rates of agglomeration.

4. Discussion

Controlled agglomeration offers the advantage of tailoring material properties to meet specific performance requirements. For instance, as agglomeration increases, particle-to-particle distances shorten, intensifying magnetic dipole interparticle interactions. This results in a more pronounced ferromagnetic

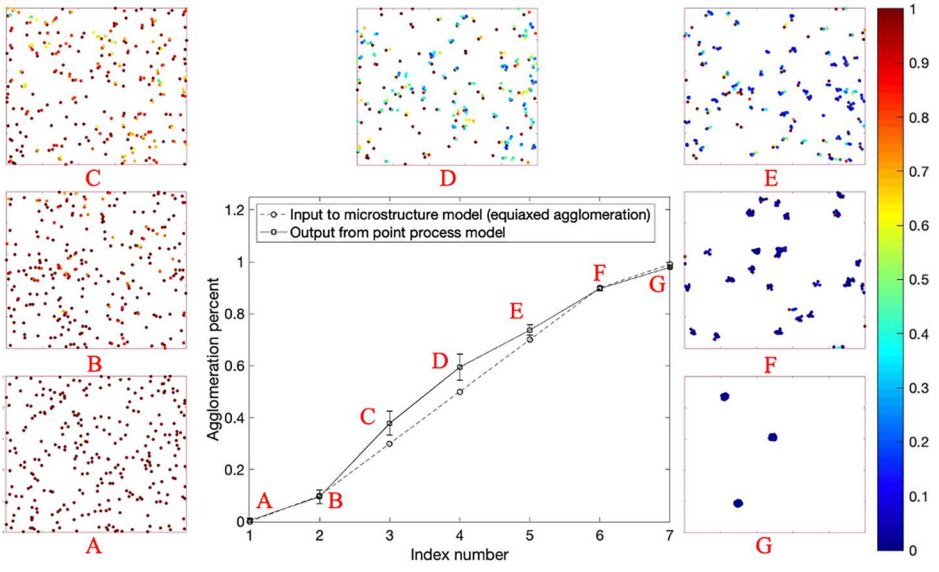

Figure 13. Comparison of percentage of agglomerated microstructure generated from stochastic model with the point process model.

behaviour with hysteresis losses, valuable for tumour treatment by selectively targeting cancer cells without harming surrounding healthy tissue [43]. Conversely, nanoparticle agglomeration can diminish the potential improvement in mechanical properties in nanocomposites due to restricted interfacial area. In orthopaedic applications [44], ceramic nanoparticles inherent

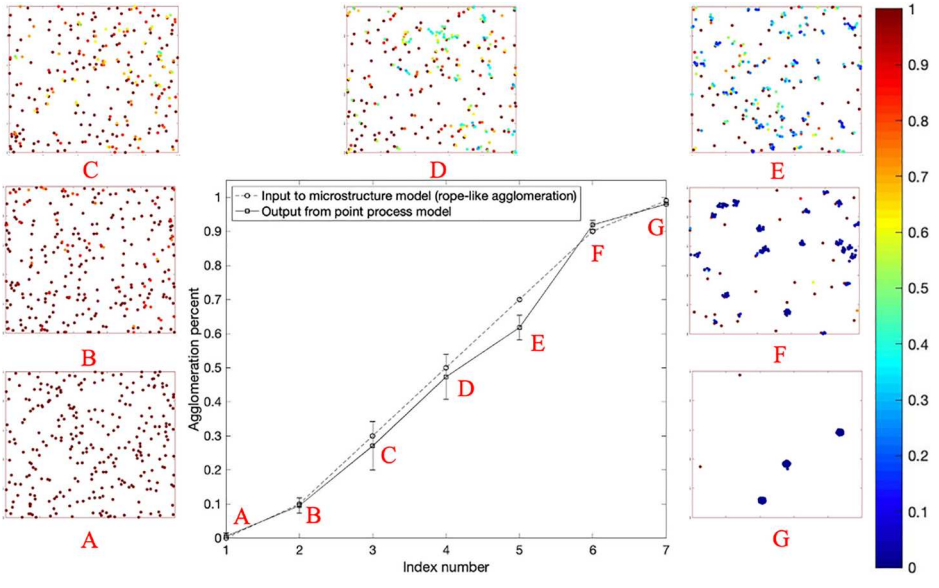

Figure 14. Comparison of percentage of rope-like agglomerated microstructure generated from stochastic model with the point process model.

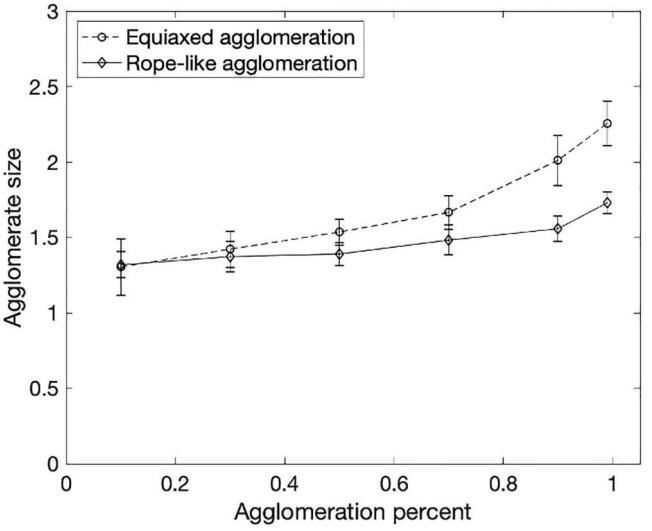

Figure 15. The average agglomeration size with error bars is represented for equiaxed and rope-like agglomerate with respect to agglomeration percent.

tendency to form larger agglomerates in a polymer matrix compromise mechanical performance. In materials' microstructure characterisation, nanoparticles have played an important role in determining strain maps and finding strain localisations via digital image correlation (DIC). In this case, properly dispersed particles must cover the area of interest, allowing the construction of displacement fields [45, 46]. The growing use of nanoparticles in everyday products raises concerns about their release into water sources and wastewater. In water treatment and wastewater sludge, nanoparticles and agglomerates with particle sizes less than 100 nm can be slow settling, prolong suspension, and hinder effective removal, increasing the risk of environmental toxicity [47]. Agglomerated nanoparticles often possess reduced effective surface areas compared to individual dispersed nanoparticles, limiting reactivity critical in applications like catalysis [48]. Additionally, agglomerates may exhibit diminished mobility and diffusion rates, impacting their effectiveness in applications requiring free nanoparticle movement, such as drug delivery [49]. Therefore, it is of utmost importance to gain a comprehensive understanding of nanoparticle behaviour with regard to aspects such as morphology, agglomeration percentage, agglomeration size, and associated factors.

Mathematical models to describe and predict nanoparticle agglomeration provide invaluable insights into the complex dynamics of nanoparticles coming together, forming clusters, and influencing various material properties. Several modelling approaches including stochastic percolation models [50], fractal analysis [51], Smoluchowski equation [52] and Kinetic Monte Carlo [53] have been used to study agglomeration. These models describe how

nanoparticles come together and form aggregates over time, taking into account factors such as particle concentration, collision frequency, and the probability of aggregation. Despite these developments, there is a limited correlation between modelling and experimental studies. Furthermore, there is a lack of modelling approaches that can quantitatively analyse a given experimental or simulated microstructure for agglomeration characteristics. The point process model proposed in this study effectively addresses this aspect.

Statistical methods offer distinct advantages in quantifying the agglomeration phenomenon compared to analytical methods. Considering the inherent stochasticity of agglomeration processes, statistical methods provide a robust framework for analysing and interpreting data. Unlike analytical techniques, statistical methods allow researchers to not only describe the central tendencies of agglomeration phenomena but also assess the variability, distribution, and trends within datasets, as well as quantify uncertainties and reveal patterns and correlations that might be overlooked by purely analytical methods. Self-exciting point process is an effective approach to model discrete history-dependent interrelated spatio-temporal events or points. Consequently, it has been used extensively in various domains with such data including earthquake occurrences [35], epidemiology[28], crime [26], financial markets [54], etc.

Despite the success of Hawkes point process models in various domains, they have not been utilised in materials science. To our knowledge, this study represents the first application of the Hawkes point process model to a problem in materials science. Self-excitation point process models are well-suited for analysing agglomeration due to the following reasons: (a) Discretisation: Point process models handle discrete points or events in the spatiotemporal domain. In the context of agglomeration, these discrete points can represent individual nanoparticles which are either dispersed or in clusters. (b) History or Path Dependence: Another prerequisite for applying point process models is the history dependence of the events or points. Agglomeration processes inherently exhibit history dependence, meaning the current state of agglomeration is influenced by the existing locations of the particles. The applied model uses a 2D dataset but holds the potential for adaptation to 3D datasets. For adapting to 3D, one would use volumetric data and convert x, y, and z positions to distance from origin in sub cells. This would be similar to the procedure described in section 2.3 except for including volumetric slices instead of planar segments. However, this would complicate the model and require 3D characterisation data. Some of the techniques used for 3D characterisation of nanoparticles include X-ray computed microtomography [55], confocal laser scanning microscopy [56] and transmission electron microscopy [57].

We acknowledge the limitations of optical microscopy, particularly when working with complex structures in three dimensions. Optical microscopy, while valuable for visualizing particle distributions, has inherent resolution limits that can introduce uncertainties in size measurements and the detailed

characterisation of nanoparticle agglomerates. These uncertainties primarily arise from diffraction limits and the inability to resolve features below the wavelength of light used in the microscope. Therefore, we complemented optical microscopy with Scanning Electron Microscopy (SEM) and Dynamic Light Scattering (DLS) spectroscopy to characterize the particle size distributions for high ultrasonication times. Another limitation is with respect to particle count. In the microstructures we have considered, the particle count varies from 621 to 89. The background rate used in the calculation is dependent on the number of particles. It is always desirable to analyse microstructures with a larger number of particles.

Here we have quasi-statically analysed the agglomeration in microstructures. The model and methodology are highly adaptable and can be readily extended to accommodate dynamic processes. For instance, the analysis in Figure 8, presents an opportunity to explore the spatiotemporal evolution of microstructures under the influence of sonication. By transitioning from quasi-static analysis to dynamic analysis, one can examine how microstructures change over time as a result of sonication. This will facilitate the time-dependent behaviour and responses of such structures and applications. Furthermore, many phenomena in material science can be discretised and have path dependence. For example, nucleation growth processes like solidification and equilibrium phase transformations. The self-excitation point process models can potentially be used for analysing such processes.

5. Conclusion

This study presents an innovative application of the self-exciting point process model to investigate nanoparticle agglomeration. Experimentally generated titanium nanoparticle microstructures were analysed, revealing a direct correlation between sonication duration and nanoparticle agglomeration. With increasing sonication time, it was observed that a simultaneous reduction in both agglomeration percentage and size. Additionally, our analysis extends to simulated carbon nanotube microstructures, encompassing a wide range of agglomeration patterns, including equiaxed and rope-like morphologies. The outcomes derived from the point process model align closely with those obtained from the microstructure model. Agglomeration size consistently increases alongside the agglomeration percentage for equiaxed and rope-like agglomerates, with equiaxed structures displaying larger agglomerates due to their star-like shape, while rope-like agglomerations are defined by their fibre-like structure. This study demonstrates that self-exciting point process models can be used for analysing phenomenon in materials science that can be broken down into discrete events or points, and exhibit path dependence. While we focus on agglomeration in this study, the approach can potentially be extended to other nucleation and growth-type processes.

Acknowledgement

This material is based upon work supported in part by the National Science Foundation under Grant numbers 2001038 and 2050887. The opinions, findings, conclusions, or recommendations expressed are those of the author(s) and do not necessarily reflect the views of the National Science Foundation.

Disclosure statement

No potential conflict of interest was reported by the author(s).

Funding

This work was supported by National Science Foundation [Grant Number 2001038, 2050887].

Data availability statement

We have added the supplemental data including microstructure images and computational codes to a GitHub repository. It can be accessed through the following link https://github.com/AMMG-at-ERAU/Nanoparticle-Agglomeration.

References

[1] I. Chowdhury, S.L. Walker, and S.E. Mylon, *Aggregate morphology of nano-TiO2: role of primary particle size, solution chemistry, and organic matter*. Environ. Sci: Processes Impacts 15 (2013), pp. 275–282.

[2] Y. Nur, J.R. Lead, and M. Baalousha, *Evaluation of charge and agglomeration behavior of TiO2 nanoparticles in ecotoxicological media*. Sci. Total Environ. 535 (2015), pp. 45–53.

[3] M. Zareei, H. Yoozbashizadeh, and H.R. Madaah Hosseini, *Investigating the effects of pH, surfactant and ionic strength on the stability of alumina/water nanofluids using DLVO theory*. J. Thermal Anal. Calorimet. 135 (2019), pp. 1185–1196.

[4] J. Jiang, G. Oberdörster, and P. Biswas, *Characterization of size, surface charge, and agglomeration state of nanoparticle dispersions for toxicological studies*. J. Nanoparticle Res. 11 (2009), pp. 77–89.

[5] K. Suttiponparnit, J. Jiang, M. Sahu, S. Suvachittanont, T. Charinpanitkul, and P. Biswas, *Role of surface area, primary particle size, and crystal phase on titanium dioxide nanoparticle dispersion properties*. Nanoscale Res. Lett. 6 (2011), pp. 1–8.

[6] S. Arya, P. Mahajan, S. Mahajan, A. Khosla, R. Datt, V. Gupta, S.J. Young, and S.K. Oruganti, *Review—influence of processing parameters to control morphology and optical properties of sol-gel synthesized ZnO nanoparticles*. ECS J. Solid State Sci. Technol. 10 (2021), pp. 23002.

[7] Y. Zare, *Study of nanoparticles aggregation/agglomeration in polymer particulate nanocomposites by mechanical properties*. Compos. A: Appl. Sci. Manuf. 84 (2016), pp. 158–164.

[8] R. Qiao, H. Deng, K.W. Putz, and L.C. Brinson, *Effect of particle agglomeration and interphase on the glass transition temperature of polymer nanocomposites*. J. Polym. Sci. B: Polym. Phys. 49 (2011), pp. 740–748.

[9] R.C. Murdock, L. Braydich-Stolle, A.M. Schrand, J.J. Schlager, and S.M. Hussain, *Characterization of nanomaterial dispersion in solution prior to in vitro exposure using dynamic light scattering technique*. Toxicol. Sci. 101 (2008), pp. 239–253.
[10] W.G. Shin, J. Wang, M. Mertler, B. Sachweh, H. Fissan, and D.Y.H. Pui, *Structural properties of silver nanoparticle agglomerates based on transmission electron microscopy: relationship to particle mobility analysis*. J. Nanoparticle Res. 11 (2009), pp. 163–173.
[11] A.M. Horst, A.C. Neal, R.E. Mielke, P.R. Sislian, W.H. Suh, L. Mädler, G.D. Stucky, and P.A. Holden, *Dispersion of TiO_2 nanoparticle agglomerates by* pseudomonas aeruginosa. Appl. Environ. Microbiol. 76 (2010), pp. 7292–7298.
[12] R.D. Boyd, S.K. Pichaimuthu, and A. Cuenat, *New approach to inter-technique comparisons for nanoparticle size measurements; using atomic force microscopy, nanoparticle tracking analysis and dynamic light scattering*. Colloids Surf. A: Physicochem. Eng. Asp. 387 (2011), pp. 35–42.
[13] S. Bandyopadhyay, J.R. Peralta-Videa, J.A. Hernandez-Viezcas, M.O. Montes, A.A. Keller, and J.L. Gardea-Torresdey, *Microscopic and spectroscopic methods applied to the measurements of nanoparticles in the environment*. Appl. Spectrosc. Rev. 47 (2012), pp. 180–206.
[14] E. Verleysen, P.-J. De Temmerman, E. Van Doren, M. Abi, D. Francisco, and J. Mast, *Quantitative characterization of aggregated and agglomerated titanium dioxide nanomaterials by transmission electron microscopy*. Powder Technol. 258 (2014), pp. 180–188.
[15] A. Rao, M. Schoenenberger, E. Gnecco, T. Glatzel, E. Meyer, D. Brändlin, and L. Scandella, *Characterization of nanoparticles using atomic force microscopy*. J. Phys. Conf. Ser. 61 (2007), pp. 971.
[16] Z. Jia, J. Li, L. Gao, D. Yang, and A. Kanaev, *Dynamic light scattering: A powerful tool for in situ nanoparticle sizing*. Colloids Interfaces 2023, 7(1), 15.
[17] T. Kim, C.H. Lee, S.W. Joo, and K. Lee, *Kinetics of gold nanoparticle aggregation: experiments and modeling*. J Colloid Interf. Sci. 318 (2008), pp. 238–243.
[18] H.H. Liu, S. Surawanvijit, R. Rallo, G. Orkoulas, and Y. Cohen, *Analysis of nanoparticle agglomeration in aqueous suspensions via constant-number Monte Carlo simulation*. Environ. Sci. Technol. 45 (2011), pp. 9284–9292.
[19] J. Morán, J. Yon, and A. Poux, *Monte carlo aggregation code (MCAC) part 1: fundamentals*. J. Colloid Interf. Sci. 569 (2020), pp. 184–194.
[20] A. Gbaguidi, S. Namilae, and D. Kim, *Stochastic percolation network model for hybrid nanocomposites*, in *IEEE Aerospace Conference*, IEEE, 2020. pp. 1–13.
[21] A. Gbaguidi, S. Namilae, and D. Kim, *Stochastic percolation model for the effect of nanotube agglomeration on the conductivity and piezoresistivity of hybrid nanocomposites*. Comput. Mater. Sci. 166 (2019), pp. 9–19.
[22] S. Bhoi, S. R. Kolan, Andreas Bück, and E. Tsotsas, *Population balance modeling of formation and breakage of nanoparticle agglomerates in a spouted bed*. Powder Technol. 433 (2024): 119271.
[23] J. Liao, S. Qing, X. Zhang, X. Huang, and X. Wang, *Factors that influence the aggregation structure of nanoparticles in nanofluids: A molecular dynamics simulation*. J. Molec. Liquids 368 (2022), 120716.
[24] R. Wang, S. Qian, and Z. Zhang, *Investigation of the aggregation morphology of nanoparticle on the thermal conductivity of nanofluid by molecular dynamics simulations*. Int. J. Heat Mass Transf. 127 (2018), pp. 1138–1146.
[25] A.R. Alian and S.A. Meguid, *Molecular dynamics simulations of the effect of waviness and agglomeration of CNTs on interface strength of thermoset nanocomposites*. Phys. Chem. Chem. Phys. 19 (2017), pp. 4426–4434.

[26] A. Daw and J. Pender, *An ephemerally self-exciting point process*. Adv. Appl. Probab. 54 (2022), pp. 340–403.
[27] G.O. Mohler, M.B. Short, P.J. Brantingham, F.P. Schoenberg, and G.E. Tita, *Self-exciting point process modeling of crime*. J. Am. Stat. Assoc. 106 (2011), pp. 100–108.
[28] Q. Zhao, M.A. Erdogdu, H.Y. He, A. Rajaraman, and J. Leskovec. Seismic: A self-exciting point process model for predicting tweet popularity. In Proceedings of the 21th ACM SIGKDD international conference on knowledge discovery and data mining, 2015, pp. 1513–1522.
[29] S. Meyer, L. Fahrmeir, and M. Höhle. *Spatio-temporal infectious disease epidemiology based on point processes*. Doctoral dissertation, Institut für Statistik, 2009.
[30] S. Towers, A. Gomez-Lievano, M. Khan, A. Mubayi, and C. Castillo-Chavez, *Contagion in mass killings and school shootings*. *PLoS One* 10 (2015), pp. e0117259.
[31] E.W. Fox, M.B. Short, F.P. Schoenberg, K.D. Coronges, and A.L. Bertozzi, *Modeling e-mail networks and inferring leadership using self-exciting point processes*. J. Am. Stat. Assoc. 111 (2016), pp. 564–584.
[32] V. Filimonov and D. Sornette, *Apparent criticality and calibration issues in the Hawkes self-excited point process model: application to high-frequency financial data*. Quant Finance 15 (2015), pp. 1293–1314.
[33] J. Chandrapala and T. Leong, *Ultrasonic Processing for Dairy Applications: Recent Advances*. Springer, New York, 2015.
[34] A. Gbaguidi, S. Namilae, and D. Kim, *Monte Carlo model for piezoresistivity of hybrid nanocomposites*. J. Eng. Mater. Technol. 140 (2018.
[35] Y. Ogata, Space-time point-process models for earthquake occurrences, Ann. Inst. Stat. Math. 50 (1998), Pp. 379–402.
[36] A. Rohatgi. WebPlotDigitizer User Manual Version 4.6, 2022.
[37] Y. Zhang, Y. Chen, P. Westerhoff, K. Hristovski, and J.C. Crittenden, *Stability of commercial metal oxide nanoparticles in water*. Water Res. 42 (2008), pp. 2204–2212.
[38] Y. Zhang, Y. Chen, P. Westerhoff, and J. Crittenden, *Impact of natural organic matter and divalent cations on the stability of aqueous nanoparticles*. Water Res. 43 (2009), pp. 4249–4257.
[39] P.C. Ma, N.A. Siddiqui, G. Marom, and J.K. Kim, *Dispersion and functionalization of carbon nanotubes for polymer-based nanocomposites: A review*. Compos. A: Appl. Sci. Manuf. 41(10) (2010), pp. 1345–1367.
[40] X. Zhang, Q. Li, T.G. Holesinger, P.N. Arendt, J. Huang, P.D. Kirven, T.G. Clapp, R.F. DePaula, X. Liao, Y. Zhao, L. Zheng, D.E. Peterson, and Y. Zhu, *Ultrastrong, stiff, and lightweight carbon-nanotube fibers*. Adv. Mater. 19 (2007), pp. 4198–4201.
[41] C.S. Jarali, S.R. Basavaraddi, B. Kiefer, S.C. Pilli, and Y.C. Lu, *Modeling of the effective elastic properties of multifunctional carbon nanocomposites due to agglomeration of straight circular carbon nanotubes in a polymer matrix*. J. Appl. Mech. 81(2) (2014), pp. 021010.
[42] N. Prakash and G.D. Seidel, *Electromechanical peridynamics modeling of piezoresistive response of carbon nanotube nanocomposites*. Comput. Mater. Sci. 113 (2016), pp. 154–170.
[43] C.L. Dennis, A.J. Jackson, J.A. Borchers, P.J. Hoopes, R. Strawbridge, A.R. Foreman, J. van Lierop, C. Grüttner, and R. Ivkov, *Nearly complete regression of tumors via collective behavior of magnetic nanoparticles in hyperthermia*. Nanotechnology 20(39) (2009), pp. 395103.
[44] H. Liu and T.J. Webster, *Mechanical properties of dispersed ceramic nanoparticles in polymer composites for orthopedic applications*. Int. J. Nanomed. 5 (2010), pp. 299–313.
[45] A.W. Mello, A. Nicolas, and M.D. Sangid, *Fatigue strain mapping via digital image correlation for Ni-based superalloys: The role of thermal activation on cube slip*. Mater. Sci. Eng: A 695 (2017), pp. 332–341.

[46] A.W. Mello, T.A. Book, A. Nicolas, S.E. Otto, C.J. Gilpin, and M.D. Sangid, *Distortion correction protocol for digital image correlation after scanning electron microscopy: emphasis on long duration and ex-situ experiments*. Exp. Mech. 57 (2017), pp. 1395–1409.

[47] S.K. Brar, M. Verma, R.D. Tyagi, and R.Y. Surampalli, *Engineered nanoparticles in wastewater and wastewater sludge - evidence and impacts*. Waste Manage. 30(3) (2010), pp. 504–520.

[48] F. Maillard, S. Schreier, M. Hanzlik, E.R. Savinova, S. Weinkauf, and U. Stimming, *Influence of particle agglomeration on the catalytic activity of carbon-supported Pt nanoparticles in CO monolayer oxidation*. Phys. Chem. Chem. Phys. (2005), pp. 375–383.

[49] M. Pavlin and V.B. Bregar, *Stability of nanoparticle suspensions in different biologically relevant media*. Digest J. Nanomater. Biostruct. (2012), 7(4).

[50] M. Haghgoo, R. Ansari, and M.K. Hassanzadeh-Aghdam, *The effect of nanoparticle conglomeration on the overall conductivity of nanocomposites*, Int. J. Eng. Sci. (2020), 157, 103392.

[51] V. Kanniah, P. Wu, N. Mandzy, and E.A. Grulke, *Fractal analysis as a complimentary technique for characterizing nanoparticle size distributions*. Powder Technol. 226 (2012), pp. 189–198.

[52] H.H. Liu, J. Lanphere, S. Walker, and Y. Cohen, *Effect of hydration repulsion on nanoparticle agglomeration evaluated via a constant number monte-carlo simulation*. Nanotechnology 26(4) (2015), pp. 45708.

[53] T.H. Lim, D. McCarthy, S.C. Hendy, K.J. Stevens, S.A. Brown, and R.D. Tilley, *Real-Time TEM and kinetic monte carlo studies of the coalescence of decahedral gold nanoparticles*. ACS Nano 3 (2009), pp. 3809–3813.

[54] Y. Aït-Sahalia, J. Cacho-Diaz, and R.J.A. Laeven, *Modeling financial contagion using mutually exciting jump processes*. J. Financ. Econ. 117 (2015), pp. 585–606.

[55] T. Xu, F. Li, and C. Lu, *Visualization of materials using the confocal laser scanning microscopy technique*. Chem. Soc. Rev. 49(8) (2020), pp. 2408–2425.

[56] D. Aishee, S. Gare, S. Swain, P. Bhattacharya, V. Dhyani, L. Giri, and S. Neogi. *3D imaging and quantification of PLL coated fluorescent ZnO NP distribution and ROS accumulation using laser scanning confocal microscopy*. AIChE J. 68, no. 9 (2022): e17801.

[57] A. J. Koster, U. Ziese, A. J. Verkleij, A. H. Janssen, and K. P. De Jong. *Three-dimensional transmission electron microscopy: A novel imaging and characterization technique with nanometer scale resolution for materials science*. J. Phys. Chem. B 104, no. 40 (2000): 9368-9370.